

# A 0.044-mm<sup>2</sup> 0.5-to-7-GHz Resistor-Plus-Source-Follower-Feedback Noise-Cancelling LNA Achieving a Flat NF of 3.3±0.45 dB

Haohong Yu, Yong Chen<sup>✉</sup>, Member, IEEE, Chirn Chye Boon<sup>✉</sup>, Senior Member, IEEE, Chenyang Li, Pui-In Mak<sup>✉</sup>, Senior Member, IEEE, and Rui P. Martins<sup>✉</sup>, Fellow, IEEE

**Abstract**—A wideband noise-cancelling low-noise amplifier (LNA) combining resistor feedback and source-follower feedback (SFF) is proposed. The SFF facilitates upsizing of the feedback resistor to improve the gain and noise figure (NF), without compromising the input-impedance matching. Another benefit is that the noise contributions of both the feedback resistor and noise-cancelling transistors are significantly reduced. Fabricated in 65-nm CMOS, the LNA exhibits a voltage gain of 16.8 dB, and a flat NF of  $3.3 \pm 0.45$  dB over a –3-dB bandwidth of 0.5 to 7 GHz. The power consumption is 11.3 mW at 1.2 V, and the die area is 0.044 mm<sup>2</sup>.

**Index Terms**—Noise cancelling, low-noise amplifier (LNA), source follower feedback (SFF), resistor feedback, CMOS, noise figure (NF), wideband input impedance matching.

## I. INTRODUCTION

WIDEBAND receivers are promising to support high-rate data communication [1], [2], or multiple wireless standards distributed over the sub-6-GHz RF spectrum [3]–[6]. Especially in the ultra-scale CMOS technologies, the transistor features an adequate  $f_T$  to serve as a wideband RF low-noise amplifier (LNA) with high gain, low noise figure (NF) and good linearity [2]–[14]. A single-transistor LNA with resistive

Manuscript received November 13, 2017; revised February 2, 2018; accepted May 3, 2018. Date of publication May 7, 2018; date of current version December 20, 2018. This work was supported by the Singapore Ministry of Education Academic Research Fund Tier 1 under Grant MOE RG86/16. This brief was recommended by Associate Editor V. Saxena. (*Corresponding author: Yong Chen.*)

H. Yu, C. C. Boon, and C. Li are with the School of Electrical and Electronic Engineering, Nanyang Technological University, Singapore 639798 (e-mail: yuhao012@e.ntu.edu.sg).

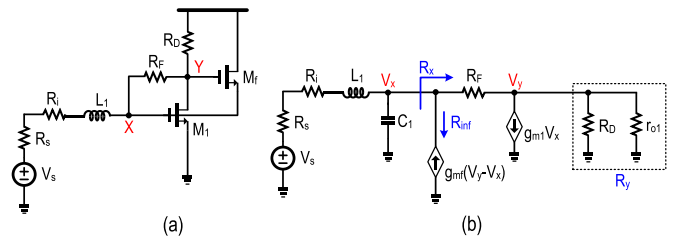
Y. Chen is with the State-Key Laboratory of Analog and Mixed-Signal VLSI, University of Macau, Macau 999078, China (e-mail: ychen@umac.mo).

P.-I. Mak is with the State-Key Laboratory of Analog and Mixed-Signal VLSI, University of Macau, Macau 999078, China, and also with the Faculty of Science and Technology, Department of ECE, University of Macau, Macau 999078, China (e-mail: pimak@umac.mo).

R. P. Martins is with the State-Key Laboratory of Analog and Mixed-Signal VLSI, University of Macau, Macau 999078, China, with the Faculty of Science and Technology, Department of ECE, University of Macau, Macau 999078, China, and also on leave from Instituto Superior Técnico, Universidade de Lisboa, 1049-001 Lisbon, Portugal (e-mail: rmartins@umac.mo).

Color versions of one or more of the figures in this paper are available online at <http://ieeexplore.ieee.org>.

Digital Object Identifier 10.1109/TCSII.2018.2833553



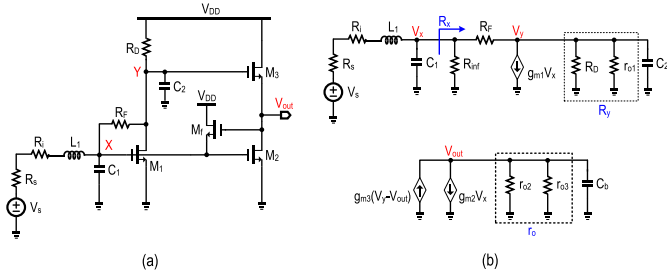


Fig. 2. (a) Schematic and (b) small-signal equivalent circuit of the proposed LNA combining local source-follower-based feedback with noise-cancelling technique.

where \$L\_1\$ is the matching inductor, \$R\_i\$ is its parasitic resistance, \$C\_1\$ is the parasitic capacitance at X and \$R\_x\$ is the resistance looking into X in Fig. 1(b). Due to the addition of SFF, \$R\_x\$ in Fig. 1(b) is expressed as

$$R_x = \frac{(R_y + R_F)R_{inf}}{(g_{m1}R_y + 1)R_{inf} + R_y + R_F} \quad (2a)$$

where

$$R_{inf} = \frac{1}{g_{mf}(1 - V_y/V_x)} \quad (2b)$$

and \$R\_y = R\_D || r\_{01}\$ as shown in Fig. 1(b). \$R\_x\$ is smaller than the typical resistive-feedback LNA due to the term \$R\_y + R\_F\$ in the denominator. Since \$V\_y/V\_x\$ is negative, it leads to a negative \$g\_{mf}(V\_y - V\_x)\$. Thus, a small-signal current in \$M\_f\$ flows from X to ground, making \$M\_f\$ an effective resistor (\$R\_{inf}\$), lowering the input impedance of the LNA. Thus, a larger \$R\_F\$ can be employed without compromising input matching. A larger \$R\_F\$ benefits both the gain and NF, as detailed later.

### B. Frequency Response of \$S\_{21}\$

Noise-cancelling technique is common in a wideband LNA to improve the NF and gain. Fig. 2(a) and (b) show, respectively, the schematic (without DC bias network) and small-signal equivalent circuit of the proposed LNA with a source follower (\$M\_f\$) and noise-cancelling paths (\$M\_2\$ and \$M\_3\$). \$C\_1\$ and \$C\_2\$ represent the total parasitic capacitances at X and Y, respectively. The total voltage gain consists of two parts: \$A\_1 = V\_x/V\_s\$ and \$A\_v = V\_{out}/V\_x\$. \$A\_1\$ is the voltage gain from the source to X, which can be written as

$$A_1 = \frac{R_x}{L_1 C_1 R_x s^2 + [L_1 + C_1 R_x (R_s + R_i)]s + R_s + R_x + R_i} \quad (3)$$

where \$R\_x\$ is given by (2a). Yet, the resistance looking into the source of \$M\_f\$ is slightly changed, \$R\_{inf} = 1/g\_{mf}(1 + |A\_v|)\$. From (3), the reactive components that mainly determine the poles of \$A\_1\$ are \$C\_1\$ and \$L\_1\$. Typically \$C\_2 \ll C\_1\$ since \$M\_3\$ is designed smaller than \$M\_1\$ and \$M\_2\$ for noise-cancelling purpose. The effect of \$C\_2\$ on \$A\_1\$ is neglected for simplicity. The second part (\$A\_v\$) of the overall LNA gain is the voltage gain from X to the output node and is given by

$$A_v = -\frac{(-g_{m3}A_2 + g_{m2})(r_0||C_b)}{1 + g_{m3}(r_0||C_b)} \quad (4a)$$

where

$$A_2 = \frac{V_y}{V_x} = -\frac{R_F R_y g_{m1} - R_y}{C_2 R_F R_y s + R_y + R_F} \quad (4b)$$

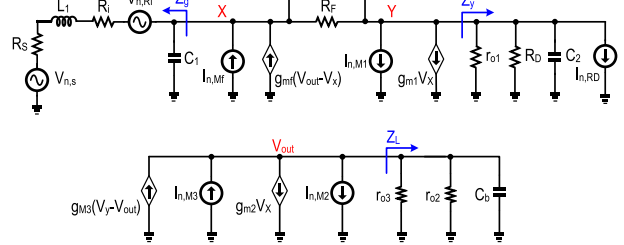


Fig. 3. Equivalent circuit of Fig. 2(a) for noise calculation.

and \$r\_0 = r\_{02}||r\_{03}\$. \$A\_2\$ is the voltage gain from X to Y. \$g\_{m2}\$, \$g\_{m3}\$, \$r\_{02}\$ and \$r\_{03}\$ are the transconductance of \$M\_2\$ and \$M\_3\$ and drain-source resistance of \$M\_2\$ and \$M\_3\$, respectively. \$C\_b\$ is the gate capacitance of the testing buffer. If we assume \$1 + g\_{m3}r\_0 \approx g\_{m3}r\_0\$, which is usually the case, (4a) can be simplified as \$A\_v = A\_2 - g\_{m2}/g\_{m3}\$. Note that \$A\_2\$ is negative and it is clear that the noise-cancelling technique also improves the gain. \$S\_{21}\$ is twice the gain in a 50-\$\Omega\$ system with impedance matching and it is given by

$$S_{21} = 2A_{core} = 2A_1 A_v \quad (5)$$

where \$A\_{core}\$ is the total voltage gain from the source to the output in Fig. 2, and \$A\_{core} = A\_v A\_1\$. Equations (2), (3) and (4) show that adding \$M\_f\$ only affects \$A\_1\$ and has no influence on \$A\_v\$. Under an matched input-impedance, i.e., \$A\_1 = 0.5\$ at DC, \$S\_{21}\$ has the same expression for both situations with and without \$M\_f\$. However, with the presence of \$M\_f\$, \$R\_F\$ can be upsized when comparing it with the non-feedback case. Thus, from (4), a larger \$R\_F\$ benefits the gain.

### C. Frequency Response of NF

The main noise sources of the LNA are the channel resistance thermal noises from \$M\_1\$, \$M\_2\$, \$M\_3\$ and \$M\_f\$, as well as the thermal noises from \$R\_D\$ and \$R\_F\$. The noise contributed by the input inductor parasitic resistance \$R\_i\$ is also taken into account. Fig. 3 shows the small-signal equivalent circuit of Fig. 2(a) for noise calculation. The noise factor of \$M\_1\$ is given by

$$F_{M1} = \frac{g_{m1}}{R_s |A_{core}|^2 \alpha} \left| \frac{R_F A_{v,n1}}{\left(1 + \frac{R_F}{Z_y}\right) A_{1,n1} + R_F g_{m1} - 1} \right| \quad (6a)$$

where

$$A_{1,n1} = \frac{V_{y,n1}}{V_{x,n1}} = 1 + \frac{R_F}{Z_g} + g_{mf} R_F \frac{\frac{g_{m2}}{g_{m3}} + \frac{1}{g_{m3} Z_L} - \frac{R_F}{Z_g}}{1 + \frac{1}{g_{m3} Z_L} + R_F g_{mf}} \quad (6b)$$

$$A_{v,n1} = \frac{V_{out,n1}}{V_{x,n1}} = \frac{g_{mf} R_F + \frac{R_F}{Z_g} + 1 - \frac{g_{m2}}{g_{m3}}}{g_{mf} R_F + \frac{1}{Z_L g_{m3}} + 1} \quad (6c)$$

As shown in Fig. 3, \$Z\_y = R\_y/(C\_2 R\_y s + 1)\$, \$Z\_L = r\_0/(C\_b r\_0 s + 1)\$, and \$Z\_g = (L\_1 s + R\_s + R\_i)/(L\_1 C\_1 s^2 + C\_1 (R\_s + R\_i)s + 1)\$. \$Z\_y\$ is the impedance of \$R\_y\$ parallel with \$C\_2\$. \$Z\_g\$ is the impedance looking into the matching network from X. \$Z\_L\$ is the total impedance at \$V\_{out}\$. \$A\_{1,n1}\$ is the ratio of noise voltage caused by \$M\_1\$ at Y to that at X. \$A\_{v,n1}\$ is the ratio of noise voltage caused by \$M\_1\$ at \$V\_{out}\$ to that at X. \$\gamma\$ is the coefficient of channel noise and \$\alpha = g\_{m1}/g\_{d0}\$, where \$g\_{d0}\$ is zero-bias drain conductance. Equation (6c) shows that perfect noise cancelling

is achieved when  $g_{mf}R_F + R_F/Z_g + 1 = g_{m2}/g_{m3}$ , leading to  $F_{M1} = 0$ . However, since  $Z_g$  is complex and  $g_{m2}/g_{m3}$  is real, a perfect noise cancellation cannot be accomplished. A good approximation is  $\Re(g_{mf}R_F + R_F/Z_g + 1) = g_{m2}/g_{m3}$ . As shown in Fig. 3, both  $I_{n,RD}$  and  $I_{n,M1}$  flow from node Y to ground, therefore the transfer functions from  $I_{n,M1}$  and  $I_{n,RD}$  to the output are the same. Both  $I_{n,M2}$  and  $I_{n,M3}$  flows from  $V_{out}$  to ground, so a similar case is true for  $I_{n,M2}$  and  $I_{n,M3}$ . Then, the noise factor of  $R_D$ ,  $M_2$  and  $M_3$  will become:

$$F_{RD} = \frac{1}{R_D g_{m1}} F_{M1} \quad (7)$$

$$F_{M2} = \frac{g_{m2}}{R_s |A_{core}|^2 \alpha} \times \left| Z_L - \frac{g_{m3}Z_L(A_{v,n2} - A_{1,n2}) + g_{m2}Z_L}{g_{m3}Z_L(A_{v,n2} - A_{1,n2}) + g_{m2}Z_L + A_{v,n2}} \right|^2 \quad (8a)$$

where

$$A_{1,n2} = \frac{V_{y,n2}}{V_{x,n2}} = -\frac{R_y(R_F g_{m1} - 1)}{C_2 R_F R_y s + R_F + R_y} \quad (8b)$$

$$A_{v,n2} = \frac{V_{out,n2}}{V_{x,n2}} = 1 + \frac{1}{g_{mf}} \frac{L_1 C_1 s^2 + C_1 R_s s + 1}{L_1 s + R_s} + \frac{1}{g_{mf}} \frac{C_2 R_y s + R_y g_{m1} + 1}{C_2 R_F R_y s + R_F + R_y} \quad (8c)$$

$$F_{M3} = \frac{g_{m3}}{g_{m2}} F_{M2} \quad (9)$$

$V_{x,n2}$ ,  $V_{y,n2}$ , and  $V_{out,n2}$  are the noise voltages caused by  $M_2$  at X, Y and  $V_{out}$ , respectively. To analyze the effect of feedback on  $F_{M2}$ , the noise factor contributed by  $M_2$  under non-feedback condition can be calculated as

$$F_{M2,wofb} = \frac{g_{m2}}{R_s |A_{core,wofb}|^2 \alpha} |Z_L|^2 \quad (10)$$

Since  $A_{1,n2}$  is negative and  $|A_{core}| > |A_{core,wofb}|$ ,  $F_{M2}$  and  $F_{M3}$  are reduced with the aid of  $M_f$ .

The noise factor contributed by feedback resistor  $R_F$  is

$$F_{RF} = \frac{1}{R_F R_s |A_{core}|^2} \cdot \left| \frac{A_{v,RF}}{\frac{1}{Z_g} + g_{mf}(1 - A_{v,RF}) + \frac{1 - A_{1,RF}}{R_F}} \right|^2 \quad (11a)$$

where

$$A_{1,RF} = \frac{V_{y,RF}}{V_{x,RF}} = -\frac{Z_y}{Z_g} - g_{m1} Z_y + g_{m3} Z_L \left( \frac{Z_y}{Z_g} + g_{m1} Z_y + 1 \right) + g_{m2} Z_L + 1 \quad (11b)$$

$$A_{v,RF} = \frac{V_{out,RF}}{V_{x,RF}} = -\frac{Z_L \left( g_{m3} \frac{Z_y}{Z_g} + g_{m1} g_{m3} Z_y + g_{m2} \right)}{1 + g_{m3} Z_L} + \frac{g_{mf} g_{m3} Z_L}{1 + g_{m3} Z_L} \frac{g_{m3} Z_L \left( \frac{Z_y}{Z_g} + g_{m1} Z_y + 1 \right) + g_{m2} Z_L + 1}{g_{m3} Z_L \left( g_{mf} - \frac{1}{Z_y} \right) - \frac{1}{Z_y}} \quad (11c)$$

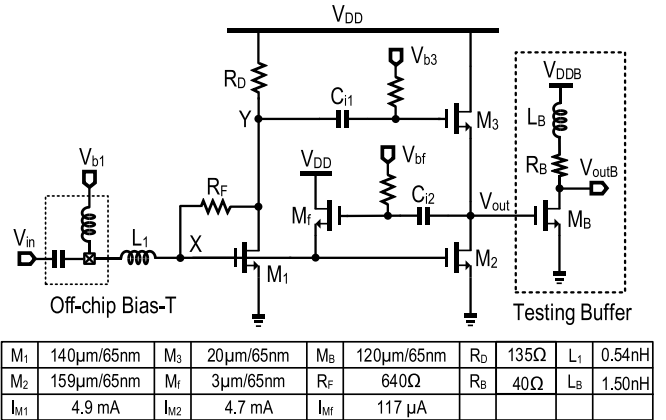


Fig. 4. Complete schematic of the proposed wideband LNA.

$V_{x,RF}$ ,  $V_{y,RF}$  and  $V_{out,RF}$  are the noise voltage caused by  $R_F$  at X, Y and  $V_{out}$ , respectively. The term  $g_{mf}(1 - A_{v,RF})$ , which is introduced by  $M_f$ , in the denominator of (11a) reduces  $F_{RF}$ . Moreover, the term  $\frac{1}{R_F} \left| \frac{A_{v,RF}}{\frac{1}{Z_g} + g_{mf}(1 - A_{v,RF}) + \frac{1 - A_{1,RF}}{R_F}} \right|^2$  decreases with increasing  $R_F$ . Since adding  $M_f$  allows larger  $R_F$  and  $|A_{core}|$ ,  $F_{RF}$  is also improved. One drawback of adding active feedback loop in LNA is the extra noise brought by  $M_f$  as given by:

$$F_{Mf} = \frac{g_{mf}}{R_s |A_{core}|^2 \alpha} \times \left| \frac{Z_g A_{v,nmf}}{(g_{mf} Z_g A_{v,nmf} - g_{mf} Z_g - 1) + \frac{Z_g (A_{1,nmf} - 1)}{R_F}} \right|^2 \quad (12a)$$

where

$$A_{1,nmf} = \frac{V_{y,Mf}}{V_{x,Mf}} = \frac{Z_y (1 - R_F g_{m1})}{R_F + Z_y} \quad (12b)$$

$$A_{v,nmf} = \frac{V_{out,Mf}}{V_{x,Mf}} = \frac{Z_L}{1 + g_{m3} Z_L} \times \frac{g_{m3} Z_y - g_{m2} Z_y - g_{m2} R_F - g_{m1} g_{m3} R_F Z_y}{R_F + Z_y} \quad (12c)$$

$V_{x,Mf}$ ,  $V_{y,Mf}$  and  $V_{out,Mf}$  are the noise voltage caused by  $M_f$  at X, Y and  $V_{out}$ , respectively.  $F_{Mf}$  increases along with  $R_F$  according to (12a). This potentially limits the improvement of NF. Yet,  $F_{Mf}$  is still buffered by an enhanced  $|A_{core}|$ . Moreover, it only contributes a small portion in total noise factor, as shown in the next section. The overall noise factor will be:

$$F = 1 + \frac{R_i}{R_s} + F_{M1} + F_{RD} + F_{M2} + F_{M3} + F_{RF} + F_{Mf} \quad (13)$$

By noise cancellation, the noise from  $M_1$  and  $R_D$  is reduced. Also, all  $F_{RF}$ ,  $F_{M2}$  and  $F_{M3}$  are decreased due to local SFF.

### III. PROPOSED COMPLETE LNA

Fig. 4 shows the complete schematic of the LNA, where we used capacitors  $C_{i1}$  and  $C_{i2}$  for DC-decoupling and voltages  $V_{b3}$  and  $V_{bf}$  to bias the transistors  $M_3$  and  $M_f$ , respectively. The gate bias ( $V_{b1}$ ) of  $M_1$  and  $M_2$ , provided by an off-chip bias-T, also biases the source of  $M_f$ . The DC current of  $M_f$  flows from  $V_{DD}$  to  $V_{b1}$ . A common-source output buffer is added to provide output matching for measurements. An inductor

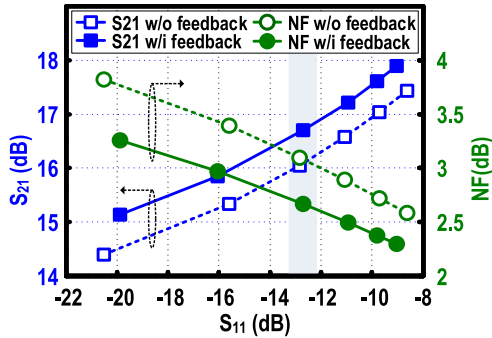


Fig. 5. Simulated NF and  $S_{21}$  versus  $S_{11}$  of the LNAs with and without the local SFF at 3 GHz.

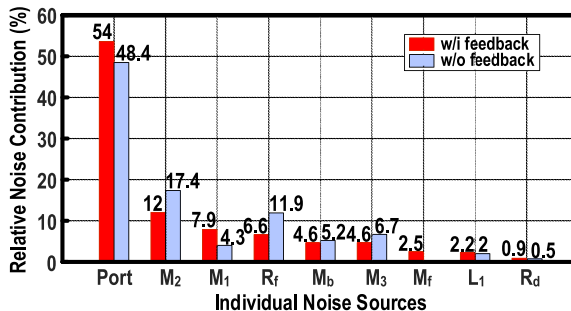


Fig. 6. Simulated relative noise contributions by individual components in the LNAs with and without local SFF.

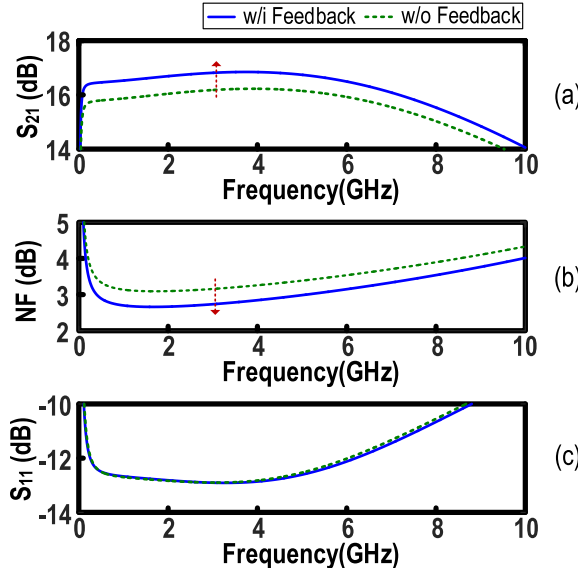


Fig. 7. Simulated (a)  $S_{21}$  and (b) NF versus frequency of the LNAs with and without local SFF, under the same (c) input matching condition.

$L_B$  is series connected to the drain of the buffer transistor to counter the effect of the load capacitance on LNA core's bandwidth. Simulations are performed to verify the performance enhancement introduced by  $M_f$ . Fig. 5 illustrates the circuit performance of the LNA with and without feedback at various  $S_{11}$ .  $R_F$  is swept to obtain the various matching conditions. The maximum improvement of gain and NF are 0.9 and 0.57 dB, respectively. Across a wide range of matching conditions, from  $-20$  to  $-8$  dB, the proposed LNA with feedback always has

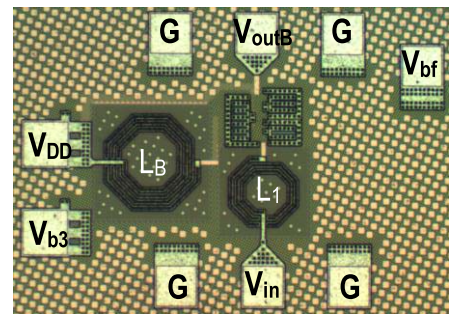


Fig. 8. Die photo of the proposed LNA.

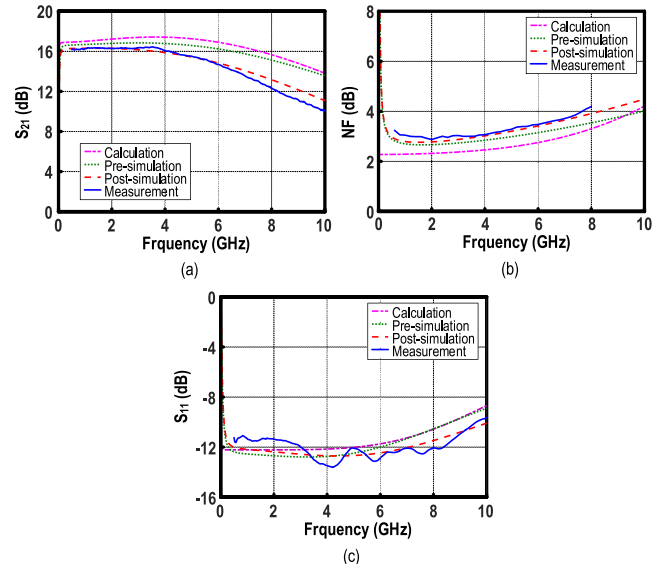


Fig. 9. Calculated, simulated and measured (a)  $S_{21}$ , (b) NF and (c)  $S_{11}$  versus frequency of the proposed LNA. Pre-simulation is pre-layout simulation and post-simulation is post-layout simulation considering the parasitic effects.

a better  $S_{21}$  and NF than the LNA without feedback. The feedback loop is unconditionally stable in the simulations.

Fig. 6 presents the relative noise contributions by individual components in the LNA with and without feedback. With  $M_f$ , the noise contribution percentages of  $M_2$ ,  $R_F$ , and  $M_3$  drop from 17.4%, 11.9% and 6.7% to 12.0%, 6.6% and 4.6%, respectively. The reduction of noise contribution is consistent with the analysis in Section II. The noise from  $M_f$  is 2.5%, which is relatively small when compared with the total noise reduction in other components. Although noise from  $M_1$  is higher than the non-feedback situation, adding  $M_f$  into the LNA improves the overall NF, which is reflected by the port noise contribution. Fig. 7 shows, at the same input matching of  $-12.5$  dB, that the proposed LNA with feedback  $M_f$  has better  $S_{21}$  and NF performance than the LNA without feedback. When both LNAs show a  $S_{11}$  of  $-12.5$  dB,  $R_F$  in the non-feedback LNA is  $300\ \Omega$ , while  $R_F$  in our proposed LNA is  $640\ \Omega$ . As discussed in Section II, a higher  $R_F$  improves both the gain and NF.  $S_{21}$  and NF are improved by 0.7 and 0.45 dB, respectively.

#### IV. MEASUREMENT RESULTS

The LNA fabricated in 65-nm CMOS occupies a die area of  $0.25 \times 0.18\ \text{mm}^2$  (Fig. 8). It draws 11.3 mW at a single 1.2-V

TABLE I  
PERFORMANCE SUMMARY AND BENCHMARK WITH THE STATE-OF-THE-ART

	CMOS	Frequency (GHz)	BW (GHz)	Gain (dB) @ GHz	NF (dB)	NF <sub>min</sub> (dB)	IIP3 (dBm) @ GHz	Supply Voltage (V)	Power (mW)	Area (mm <sup>2</sup> )	FOM*
<b>This Work</b>	65nm	0.5 – 7	6.5	16.8 @ 4	2.87 – 3.77	2.87	-4.5 @ 4	1.2	11.3	0.044	3.57
[4] TCAS-I'12	65nm	0.1 – 5.3	5.2	10.7 @ 1	2.9 – 5.4	2.9	-6 @ 1	1	7	0.03	-3.43
[5] MWCL'15	65nm	0.1 – 2.5	2.4	18 @ 0.5	1.7 – 2.7	1.7	-3 @ 2.2	1.2	13	0.008	3.71
[6] ESSCIR'10	65nm	0.1 – 4.0	3.9	18 @ 0.5	2 – 4.4	2	-5.5 @ 1	1.2	12	0.001	1.9
[7] TCAS-II'10	90nm	3.0 – 8.5	5.5	16 @ 3	3.1 – 4.4	3.1	-5.4 @ 5	1.2	16	0.022	-4.43
[8] JSSC'10	130nm	2.1 – 3.4	1.3	16.4 @ 0.7	2.1 – 3.4	2.1	0 @ 0.9	1.8	14.4	0.036	-1
[11] TMTT'16	130nm	0.1 – 2.2	2.1	12.3 @ 0.2	4.9 – 6	4.9	-10.5 @ 1	1	0.4	0.005	-0.70
[12] TMTT'10	180nm	1.7 – 5.9	4.2	13.5 @ 3.5	3.6 – 4.7	3.6	-12 @ 6	1.8	10.34	0.565	-20.5
[13] TCAS-II'13	180nm	0.5 – 1.3	0.8	10 @ 0.6	2.9 – 3.2	2.9	7.5 @ 1	2	18	0.07	-1.6
[14] MWCL'14	180nm	dc – 1.4	1.4	16.4 @ 0.1	3 – 4.7	3	-11 @ 0.9	1.8	12.8	0.04	-24
[3] JSSC'04	250nm	0.02 – 1.6	1.6	13.7 @ 0.01	1.9 – 2.2	1.9	0 @ 0.9	1.6	28.5	0.043	-6.1

$$^* FOM = 20 \log_{10} \left( \frac{IIP3[mW] \times Gain[lin] \times BW[GHz]}{P_{dc}[mW] \times (NF[lin]-1)} \right) \text{ in [4].}$$

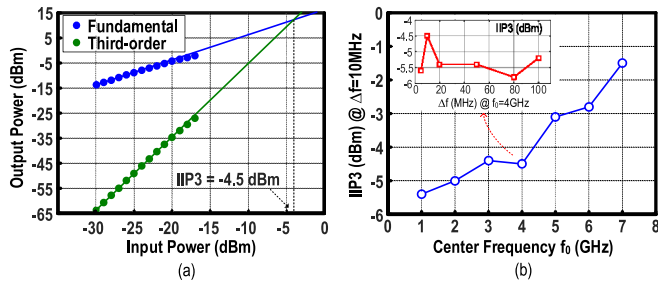


Fig. 10. (a) Measured IIP3 of the proposed LNA for two-tone inputs of 4 and 4.01 GHz and (b) Measured IIP3 versus center frequency ( $f_0$ ) and two-tone separation ( $\Delta f$ ) of the proposed LNA.

supply. Fig. 9 compares the calculated, simulated and measured results of  $S_{21}$ , NF and  $S_{11}$ . The peak  $S_{21}$  is 16.8 dB with a -3dB bandwidth ( $f_{-3dB}$ ) of 7 GHz.  $S_{21}$  has a maximum in-band ripple of 0.32 dB. Measured NF<sub>min</sub> and NF<sub>max</sub> is 2.87 dB at 2 GHz, and 3.77 dB at 7 GHz. In-band variation of NF is only 0.84 dB from 0.5 to 7 GHz. The calculated results derived in Section II are consistent with the simulated and measured results. Fig. 10(a) shows that the measured IIP3 is -4.5 dBm, when two-tone signals at 4 and 4.01 GHz are applied. The frequency spacing  $\Delta f$  between the two-tone signals at 4 GHz is swept as shown in Fig. 10(b). The highest IIP3 is -4.5 dBm when the space is 10 MHz, and the lowest IIP3 is -5.8 dBm when the space is 80 MHz. IIP3 is also measured across various center frequencies. IIP3 steadily increases with center frequency due to a lower gain at higher frequency. The highest IIP3 is -1.5 dBm at 7 GHz.

Table I benchmarks the performances with the prior art. This brief has low-and-flat NF, high gain and better overall FOM. Although inductors are applied, the area is still comparable to other works without passive inductors [4], [8], [14].

## V. CONCLUSION

This Brief has described a wideband noise-cancelling LNA using resistor plus source-follower feedback to enhance the gain and NF. The design principles and parameter tradeoff have been analyzed in detail, and the analysis is consistent with both the simulation and measurement results. The

LNA prototype fabricated in 65-nm CMOS shows a competitive performance with respect to the state-of-the-art.

## REFERENCES

- [1] S. Stroh, "Ultra-wideband: Multimedia unplugged," *IEEE Spectr.*, vol. 40, no. 9, pp. 23–27, Sep. 2003.
- [2] C.-F. Liao and S.-I. Liu, "A broadband noise-canceling CMOS LNA for 3.1–10.6-GHz UWB receivers," *IEEE J. Solid-State Circuits*, vol. 42, no. 2, pp. 329–339, Feb. 2007.
- [3] F. Brucolieri, E. A. M. Klumperink, and B. Nauta, "Wide-band CMOS low-noise amplifier exploiting thermal noise canceling," *IEEE J. Solid-State Circuits*, vol. 39, no. 2, pp. 275–282, Feb. 2004.
- [4] K.-H. Chen and S.-I. Liu, "Inductorless wideband CMOS low-noise amplifiers using noise-canceling technique," *IEEE Trans. Circuits Syst. I, Reg. Papers*, vol. 59, no. 2, pp. 305–314, Feb. 2012.
- [5] H. Lee, T. Chung, H. Seo, I. Choi, and B. Kim, "A wideband differential low-noise-amplifier with IM3 harmonics and noise canceling," *IEEE Microw. Wireless Compon. Lett.*, vol. 25, no. 1, pp. 46–48, Jan. 2015.
- [6] X. Wang, W. Aichholzer, and J. Sturm, "A resistive feedback LNA with feedforward noise and distortion cancellation," in *Proc. Eur. Solid-State Circuits Conf. (ESSCIRC)*, Sep. 2010, pp. 406–409.
- [7] M. M. Reja, K. Moez, and I. Filanovsky, "An area-efficient multistage 3.0- to 8.5-GHz CMOS UWB LNA using tunable active inductors," *IEEE Trans. Circuits Syst. II, Exp. Briefs*, vol. 57, no. 8, pp. 587–591, Aug. 2010.
- [8] Y.-H. Yu, Y.-S. Yang, and Y.-J. E. Chen, "A compact wideband CMOS low noise amplifier with gain flatness enhancement," *IEEE J. Solid-State Circuits*, vol. 45, no. 3, pp. 502–509, Mar. 2010.
- [9] W.-H. Chen, G. Liu, B. Zdravko, and A. M. Niknejad, "A highly linear broadband CMOS LNA employing noise and distortion cancellation," *IEEE J. Solid-State Circuits*, vol. 43, no. 5, pp. 1164–1176, May 2008.
- [10] B. Guo, J. Chen, L. Li, H. Jin, and G. Yang, "A wideband noise-canceling CMOS LNA with enhanced linearity by using complementary nMOS and pMOS configurations," *IEEE J. Solid-State Circuits*, vol. 52, no. 5, pp. 1331–1344, May 2017.
- [11] M. Parvizi, K. Allidina, and M. N. El-Gamal, "An ultra-low-power wideband inductorless CMOS LNA with tunable active shunt-feedback," *IEEE Trans. Microw. Theory Techn.*, vol. 64, no. 6, pp. 1843–1853, Jun. 2016.
- [12] J. Kim, S. Hoyos, and J. Silva-Martinez, "Wideband common-gate CMOS LNA employing dual negative feedback with simultaneous noise, gain, and bandwidth optimization," *IEEE Trans. Microw. Theory Techn.*, vol. 58, no. 9, pp. 2340–2351, Sep. 2010.
- [13] D. Im, "A +9dBm output P<sub>1dB</sub> active feedback CMOS wideband LNA for SAW-less receivers," *IEEE Trans. Circuits Syst. II, Exp. Briefs*, vol. 60, no. 7, pp. 377–381, Jul. 2013.
- [14] J. Y.-C. Liu, J.-S. Chen, C. Hisa, P.-Y. Yin, and C.-W. Lu, "A wideband inductorless single-to-differential LNA in 0.18  $\mu$ m CMOS technology for digital TV receivers," *IEEE Microw. Wireless Compon. Lett.*, vol. 24, no. 7, pp. 472–474, Jul. 2014.
- [15] B. Razavi, *RF Microelectronics*, 2nd ed. New York, NY, USA: Prentice-Hall, 2012, pp. 269–271.